buildings

MDPI

Article

Bonding Performance of Concrete Structure Strengthened with Ultra-High-Performance Concrete Under Bending Experiment

Chao Zhu [1], Yayi Feng [2,3], Jie Tang [1,4], Zhimei Jiang [2,3], Yinbin Li [5] and Jun Yang [2,3,*]

[1] Chongqing Design Group Co., Ltd., Chongqing 400015, China
[2] State Key Laboratory of Mountain Bridge and Tunnel Engineering, Chongqing Jiaotong University, Chongqing 400074, China
[3] School of Civil Engineering, Chongqing Jiaotong University, Chongqing 400074, China
[4] School of Civil Engineering, Chongqing University, Chongqing 400044, China
[5] Guizhou Provincial Transportation Planning Survey and Design Institute Co., Ltd., Guiyang 550081, China
* Correspondence: yangjun@cqjtu.edu.cn

Abstract: Ultra-high-performance concrete is widely used in bridge strengthening to improve mechanical performance and bridge durability. Interfacial bonding performance is a key factor in ensuring the effectiveness of ultra-high-performance concrete strengthening. The bending test of the UHPC–NC composite structure was carried out in this article. The effects of groove treatment type and epoxy resin bonding were considered to discuss the damage modes, load–deflection relationships, and strengths. The interfacial tensile strength of the UHPC–NC composite structure and the distribution pattern of cracks were clarified. The results of the test showed that (a) only 22.2% of the groove-treated specimens failed due to bonding surface failure, indicating that the UHPC–NC bonding surface has a high degree of reliability; (b) the strength of specimens with an epoxy adhesive interface was the lowest. It was only 21% higher than the pure normal concrete specimen, and the effective synergistic force of UHPC–NC cannot be achieved; (c) the specimens treated with a positive trapezoidal keyway exhibited the highest strength, with an increase of approximately 200% compared to the pure normal concrete specimens. The strength of bending specimens with right-angled and inverted trapezoidal grooves increased by approximately 100% compared with pure normal concrete specimens. Based on the established three-dimensional numerical model and the analysis of test results under economic and safe conditions, the positive trapezoidal keyway specimen exhibits superior interfacial bonding–tensile performances.

Keywords: ultra-high-performance concrete (UHPC); bridge strengthening; bending performance; interface treatment; finite element analysis

Citation: Zhu, C.; Feng, Y.; Tang, J.; Jiang, Z.; Li, Y.; Yang, J. Bonding Performance of Concrete Structure Strengthened with Ultra-High-Performance Concrete Under Bending Experiment. *Buildings* **2024**, *14*, 4040. https://doi.org/10.3390/buildings14124040

Academic Editor: Grzegorz Ludwik Golewski

Received: 14 November 2024
Revised: 10 December 2024
Accepted: 16 December 2024
Published: 19 December 2024

1. Introduction

With the rapid development of civil engineering, the demand for concrete material performance has increased. In this context, ultra-high-performance concrete (UHPC) came into being. The concept of UHPC, a new type of cement-based composite material with ultra-high strength, high toughness, and high durability, was first proposed in the 1990s by Richard et al. [1] Its appearance marks a new era in concrete technology [2–4].

The bonding interface is directly related to the permanent stability and structural safety of bridge strengthening. It is therefore essential to ensure the efficient and sustainable bonding of the strengthening interface in bridge strengthening [5–7]. UHPC is widely recognized as an effective material to enhance the performance of existing bridges due to its excellent mechanical performance and durability [8]. But the compressive strengths of UHPC and NC, which are 120–180 MPa and 20–40 MPa, respectively, are significantly different. The tensile strength of UHPC is usually between 8 and 12 MPa, while the tensile strength of NC is generally between 1.5 and 3 MPa [9]. The study of interfacial bonding performance between UHPC and normal concrete (NC) has received considerable attention [10,11].

The bending performance of the interface is an important indicator for evaluating the strengthening effectiveness of existing structures [12–14]. The performance of UHPC in bending is particularly remarkable. Numerous scholars have carried out in-depth research on the bending performance of the UHPC–NC interface. Lampropoulos [15,16] and Chen et al. [17] investigated strengthening reinforced concrete (RC) beams strengthened with UHPC by flexural loading on the specimens. The results showed that the flexural ultimate load capacity of the specimens strengthened with a three-sided jacket was increased by 53%. Farhat et al. [18] tested RC beams strengthened with thin UHPC panels, and epoxy adhesive was used for the connection between UHPC and RC beams. The failure load increased to 86%. Beschi et al. [19] investigated the application of UHPC for repairing beam-column nodes and observed a significant enhancement in load-carrying. Yang et al. [20] studied the shear behavior and strength characteristics of the UHPC–NC mesoscopic interface under the combined effect of mechanical interlocking and pin action. Tayeh et al. [21,22] formulated UHPC with a compressive strength of 170 MPa and performed split tensile tests using UHPC–NC cylindrical bonded specimens. The interfacial transition zone (ITZ) was microscopically examined by SEM/EDS scanning electron microscopy, and the bonded interface of UHPC–NC was shown to be reliable.

Similar splitting tensile test studies have been carried out by Carbonell [23], Sarkar [24], Alhallaq [25], and Li [26]. UHPC–NC prismatic bonded specimens with dimensions of 75 mm × 75 mm × 285 mm were used to conduct three-point bending tests. The results showed that the UHPC–NC bonded specimens had good integrity during the stressing process. The interfacial separation was not detected after the destruction of the specimens. This indicated that the interfacial bonding performance of UHPC–NC was good. The bending studies were carried out by Alaee [27] and Tayeh [28]. Elsaigh et al. [29] conducted a four-point bending test on the UHPC specimen. The actual mid-span moment-curvature relationship curve was obtained. The curvature measurement method was obtained per JCIS-003-2007. Schultz [30] derived a formula for calculating the tensile strength from the bending and tensile strengths of light UHPC specimens of different thicknesses. Shrinkage-cracking specimens of old and new concrete bond surfaces under different influencing parameters (e.g., environment, thickness of reinforcement layer, etc.) were studied. The effects of quantifying the separation of these factors as well as combining them were discussed by Beushausen [31]. Li et al. [32] used epoxy resin adhesive to connect a steel bar to UHPC and carried out a pull-out test. It was concluded that the tensile ratio of this specimen had a significant effect on the separation performance and tensile performance of the hybrid connection.

In summary, existing research on the bending performance of the interface between UHPC and NC predominantly builds upon studies on NC interfaces, with a strong emphasis on qualitative analysis. However, investigation into the fundamental bending performance of the UHPC–NC interface remains inadequate. To understand the bending performance of the UHPC–NC interface, a four-point bending test was carried out in this paper. By setting different connection interfaces, key indicators such as bond surface damage mode, load–deformation relationship, and bending strength were analyzed. The test results were simulated and verified by the ANSYS finite element model. The influence mechanism of interface bonding performance was further analyzed to ensure the structural safety and durability of bridge strengthening.

2. Experiment Program

2.1. Specimens

To investigate the effect of notch type on structural tensile strength and crack pattern, this paper designed and produced UHPC–NC composite specimens with dimensions of 100 mm × 100 mm × 400 mm. The thickness of the UHPC and NC layers was 30 mm and 70 mm, respectively. The three types of interface grooves were designed, i.e., positive trapezoidal, inverted trapezoidal, and right-angled. The groove bonding interface is the interface between the existing concrete and the newly poured reinforced concrete. In addition, a set of

specimens with an epoxy-bonded interface was designed to compare the bonding performance of the groove-treated interface. The specimen parameters are shown in Table 1.

Table 1. Design scheme of UHPC–NC bending specimen.

Specimen Number	Experimental Factors/mm				No. of Specimens
	Groove Depth	Groove Width	Groove Spacing	Groove Shape	
L1-1~3	10	10	100	Perpendicular type	3
L2-1	10	10	100	Positive trapezoid	1
L3-1	10	10	100	Inverted trapezoidal	1
L4-1~3	Epoxy resin adhesive bonding				3
LN-1~3	Pure NC prism specimen				3
LU-1~3	Pure UHPC prism specimen				3

The interfacial frictional resistance was greater than the tangential force along the beveled surface when the angle between the beveled edge of the trapezoidal groove and the normal bonding surface was less than 22°. The effect of stopping an interfacial slip can be achieved. Therefore, to facilitate the production of the specimen, the angle between the oblique edge of the trapezoidal grooving and the bonding surface was set to 79° [33]. The angle between the oblique edge of the inverted trapezoidal grooving and the bonding surface was set to 101°. The angle between the oblique edge of the right-angle grooving and the bonding surface was set to 90°. The detailed shape of the specimen is shown in Figure 1, and the size of the specimen is shown in Figure 2.

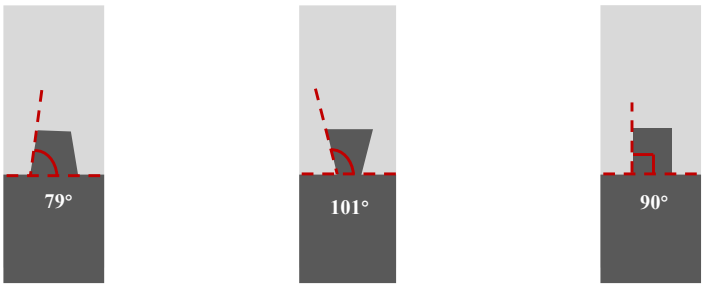

(**a**) Positive trapezoid (**b**) Inverted trapezoidal (**c**) Perpendicular type

Figure 1. Groove shape diagram.

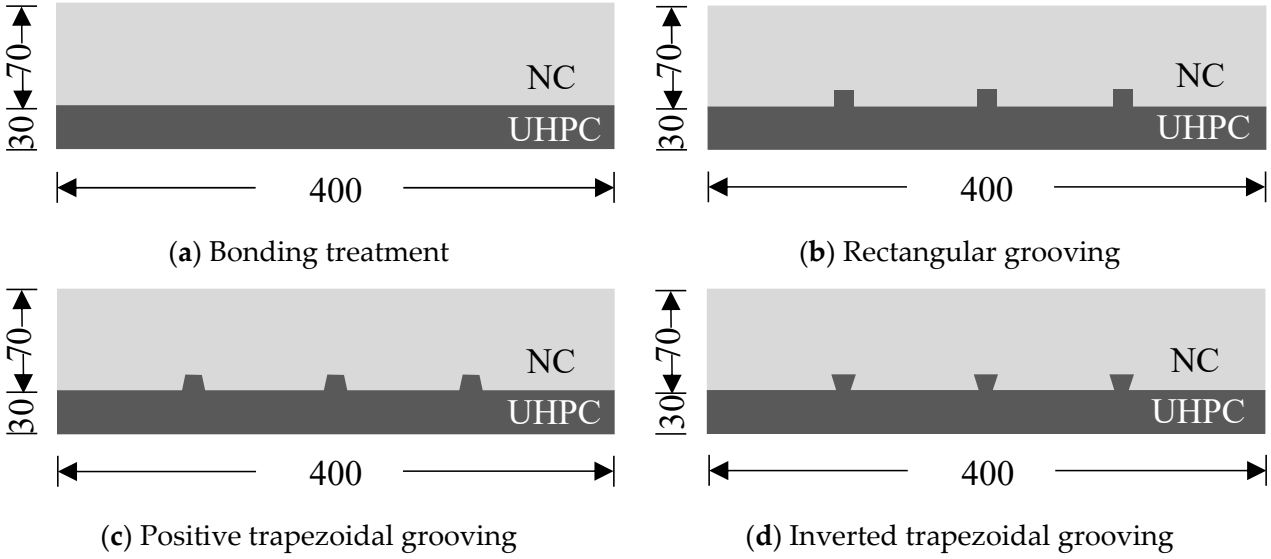

(**a**) Bonding treatment (**b**) Rectangular grooving

(**c**) Positive trapezoidal grooving (**d**) Inverted trapezoidal grooving

Figure 2. The size diagram of UHPC–NC bending specimen (mm).

2.2. Materials

2.2.1. UHPC

The composition of UHPC includes cement, silica fume, quartz sand, quartz powder, superplasticizer, and steel fiber (8 mm length and 0.12 mm diameter of straight steel fiber). The mix ratio of UHPC is shown in Table 2.

Table 2. UHPC mix ratio (kg/m^3).

Ingredient	Cement	Silica Fume	Quartz Sand	Quartz Powder	Water Reducer	Water
Unit weight	933	233	1026	280	18	210

Note: The volume content of steel fiber is 2%.

Regarding GB/T 50082-2009 [34], two sets of UHPC prisms of 100 mm × 100 mm × 515 mm were designed to measure shrinkage properties. The arrangement and results of the mechanical properties of UHPC are shown in Figure 3 and Table 3, respectively.

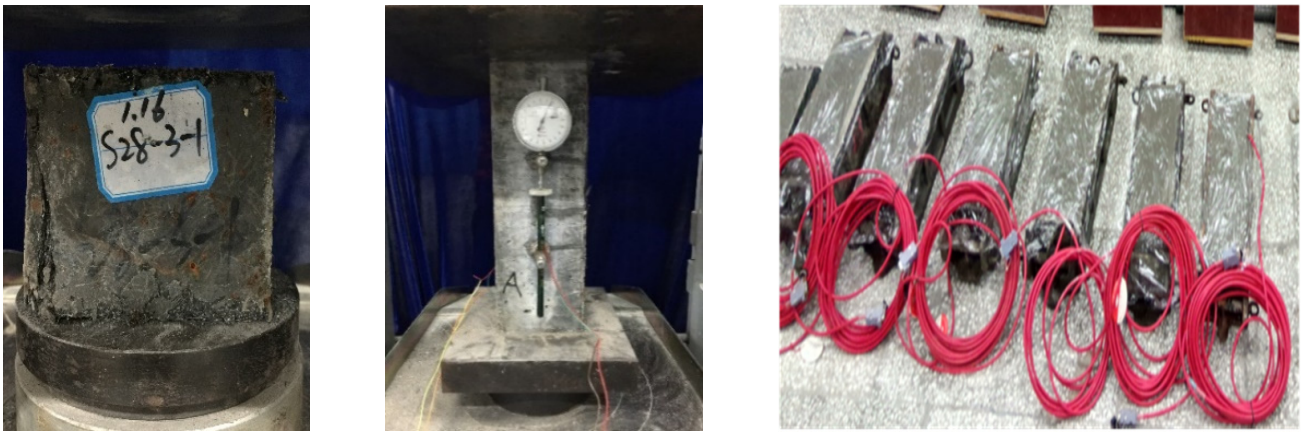

(**a**) Compressive strength (**b**) Elastic modulus (**c**) Shrinkage

Figure 3. UHPC material properties test.

Table 3. UHPC properties results.

Material	Compressive Strength/MPa	Tensile Strength/MPa	Elastic Modulus/MPa	Shrinkage
UHPC	≥150	≥9.7	≥45 × 10^3	360 με

2.2.2. Normal Concrete

The grade of NC used for the tests is C40. The mixes used are shown in Table 4.

Table 4. Mix proportion of NC (kg/m^3).

Grade	Cement	Sand	Gravel (0–10 mm)	Water	Water Cement Ratio	Percentage of Sand
C40	482	519	1272	185	0.38	29%

Substrate damage tests were performed on NC. It was found that the NC substrate damage area gradually increased with the depth, width, and number of grooves cut. The specimen design scheme is shown in Table 5.

Table 5. NC damage specimen design scheme.

Groups	Specimen Number	Experimental Factors/mm		
		Groove Depth	Groove Width	Groove Spacing
Group A	PA-1	5	20	75
	PA-2	10	20	75
	PA-3	15	20	75
Group B	PB-1	10	10	75
	PB-2	10	20	75
	PB-3	10	30	75
Group C	PC-1	10	20	50
	PC-2	10	20	75
	PC-3	10	20	100
Group D	PD-1	0	0	0
	PD-2	0	0	0
	PD-3	0	0	0

The ultimate load was recorded and the failure strength was calculated according to Equation (1):

$$f_{NC} = F/A \tag{1}$$

where f_{NC} was the destructive strength of the NC damage specimen (MPa); F was the ultimate load of the specimen (N); and A was the direct pressure area of the damaged specimen (mm^2), and the direct pressure area in the test was 50 mm × 100 mm.

To compare and analyze the ungrooved prismatic specimens, two damage evaluation indexes (volume loss rate (α) and strength loss rate (β)) were introduced. α was the ratio of the lost volume of the grooved prism to the volume of the ungrooved prism, and β was the ratio of the lost strength of the grooved prism to the strength of the ungrooved prism. They were calculated according to Equations (2) and (3).

$$\alpha = \frac{V_0 - V}{V_0} \times 100\% \tag{2}$$

$$\beta = \frac{f_{NC_0} - f_{NC}}{f_{NC_0}} \times 100\% \tag{3}$$

where V_0 was the volume of ungrooved prisms, which in this test was the volume of group D prisms; V was the volume of grooved prisms; f_{NC_0} was the strength of ungrooved prisms, which in this test was the average strength of prisms in group D, and its value was 40.54 MPa; and f_{NC} was the strength of grooved prisms.

The results of the test and the damage evaluation index results are listed in Table 6.

Table 6. NC damage test results.

Groups	Specimen Number	Loading/kN	Destructive Strength/MPa	Volumetric Loss Ratio	Strength Loss Rate
Group A	PA-1	187.49	37.50	0.03%	7.50%
	PA-2	169.85	33.97	0.06%	16.21%
	PA-3	164.62	32.92	0.09%	18.79%
Group B	PB-1	159.67	31.93	0.03%	21.23%
	PB-2	166.81	33.36	0.06%	17.71%
	PB-3	104.21	20.84	0.09%	48.59%
Group C	PC-1	126.34	25.27	0.08%	37.67%
	PC-2	189.24	37.85	0.06%	6.64%
	PC-3	176.60	35.32	0.04%	12.88%
Group D	PD-1	198.25	39.65	/	/
	PD-2	215.65	43.13		
	PD-3	194.25	38.85		

The strength loss distribution of NC specimens was plotted, as shown in Figure 4. It can be seen that the degree of strength loss of NC specimens was mostly between 10% and 20%, and only two specimens had a large degree of strength loss, with the degree of loss close to 50%.

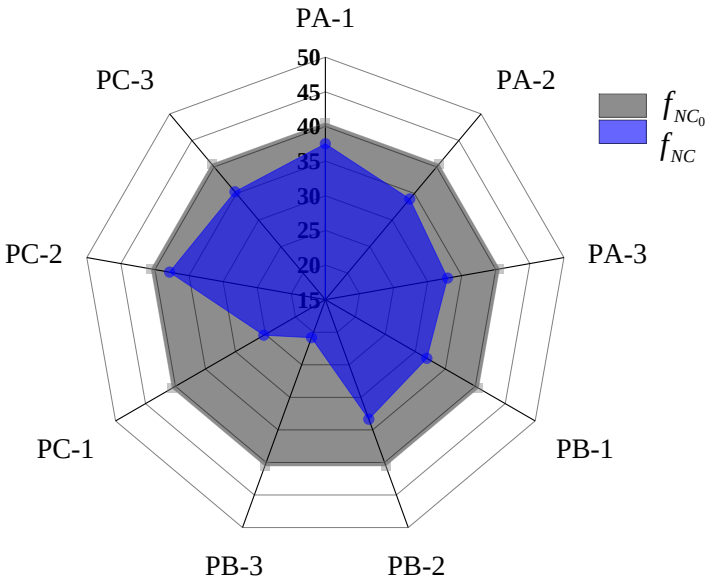

Figure 4. Strength loss distribution diagram (MPa).

When the volume loss rates of NC substrates are equal, the groove width has a more significant effect on the strength loss rate than the depth. It was recommended that the groove width be ≤20 mm to prevent the excessive strength loss of the NC matrix leading to ineffective strengthening. The NC matrix strength loss rate and the volume loss rate were positively correlated. When the volume loss rate was lower than 0.06%, the degree loss rate was lower than 20%. When the volume loss rate was higher than 0.06%, the degree loss rate increased sharply. Hence, it was recommended that the NC matrix grooving volume loss rate be ≤0.06%. The degree of the NC matrix deformation was positively correlated with the rate of volume loss, and the grooving weakened the stiffness. The loading process is shown in Figure 5.

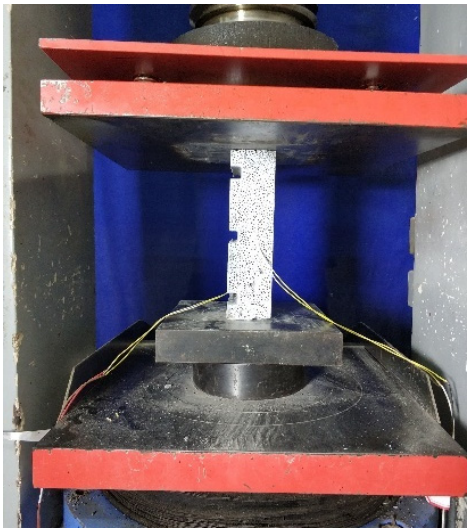

Figure 5. Loading of NC damaged specimens.

2.3. Specimen Production

(1) C40 was used to cast the NC layer in a non-standard prismatic formwork.
(2) After the NC layer specimens reached maturity, one portion was grooved while another portion was left untreated.
(3) The grooved NC layer specimens were placed back into the formwork and subsequently the UHPC layer was poured to complete the grooved set of composite specimens. Simultaneously, a portion of pure UHPC layer specimens was poured.
(4) The specimens were cured at room temperature for 24 h and then removed from the formwork. Later, 90 °C high-temperature steam curing was carried out for 48 h. Once the steam curing was complete, the specimens continued to be cured at room temperature until reaching the standard age of 7 days.
(5) The epoxy resin adhesive was used to adhere the ungrooved NC to the UHPC specimens, completing the fabrication of the adhesive group of specimens.

The specimen fabrication process is shown in Figure 6.

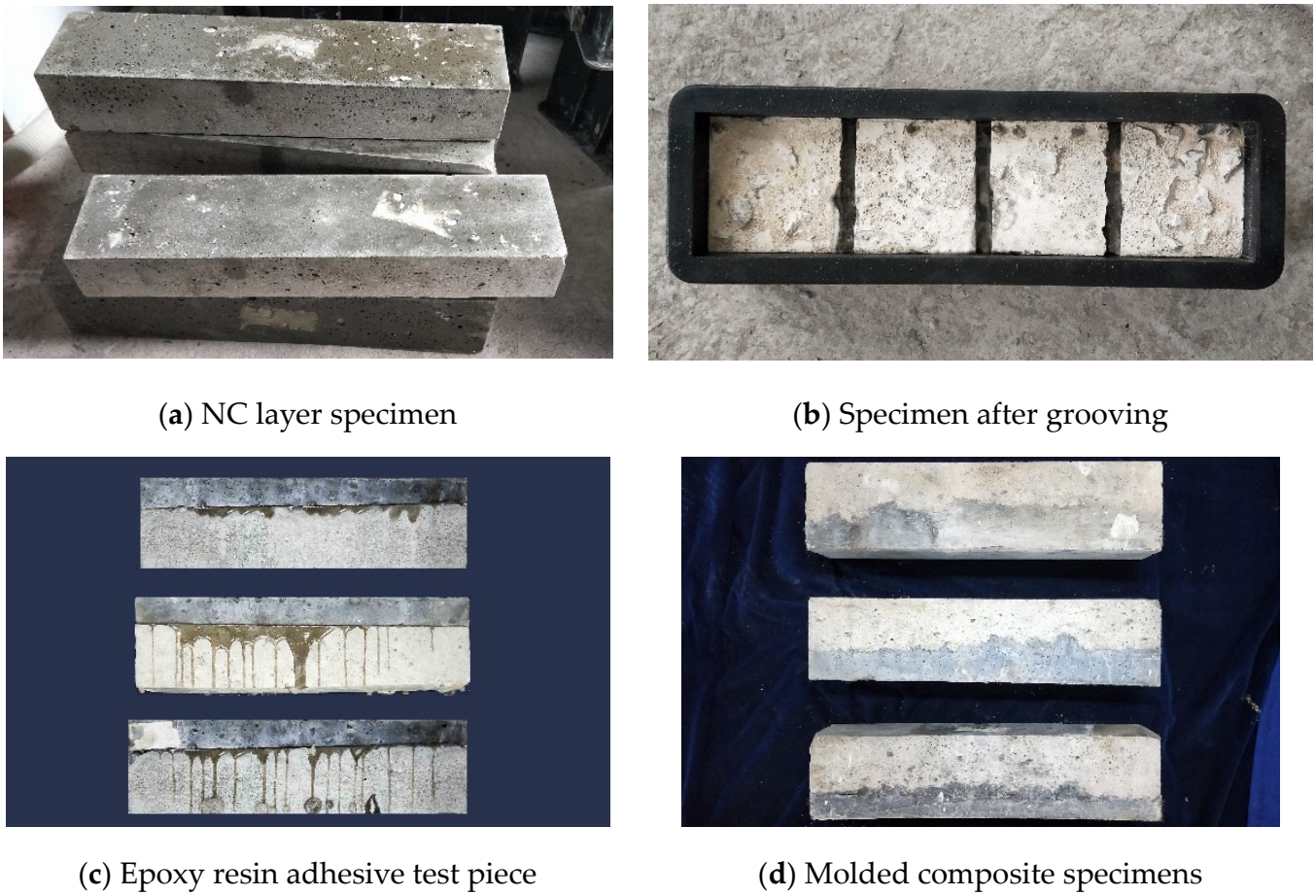

(**a**) NC layer specimen (**b**) Specimen after grooving

(**c**) Epoxy resin adhesive test piece (**d**) Molded composite specimens

Figure 6. UHPC–NC bending specimen production.

2.4. Loading and Measurement Program

A displacement gauge was arranged at the mid-span position of the specimen to measure its deformation. An MTS universal material testing machine with a range of 200 kN was used for loading at a rate of 0.1 kN/s, as shown in Figure 7.

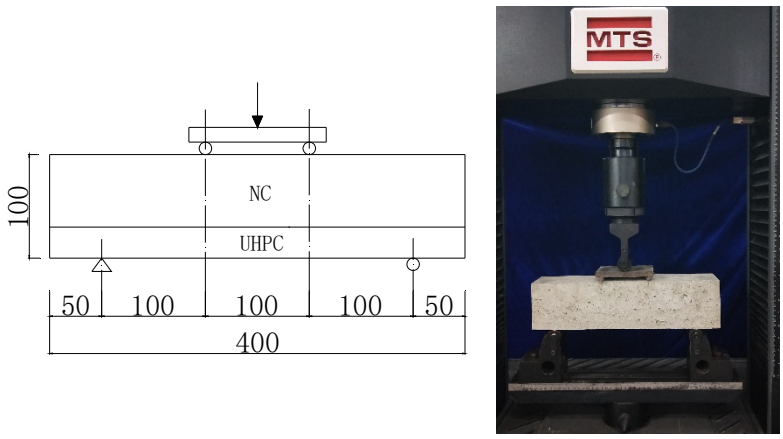

Figure 7. Test setup (mm).

3. Analysis of Results

3.1. Failure Mode

The failure mode of each group was observed after the specimens were damaged. The failure mode of each group is described in detail below.

The damage area appeared on the lower bottom surface within the two loading points. Only a few specimens showed bottom edge damage outside the region of the two concentrated load lines of action due to the occurrence of bond interface cracking. This indicated that the test effect was ideal.

(1) Groove cutting group

The damage modes of the groove-treated UHPC–NC specimens can be categorized into two types, as shown in Figure 8.

(a) Uncracked bonding surface: Cracks developed upward from the lower edge of the specimen. The area of damage on the lower bottom surface of the specimen occurred within the range of the two loading points.

(b) The cracks developed from the NC grooving location. One side progressed along the bonding surface to the end of the specimen and the other side progressed within the NC substrate to the concentrated load location. The damage location appeared outside the region of two concentrated load lines of action.

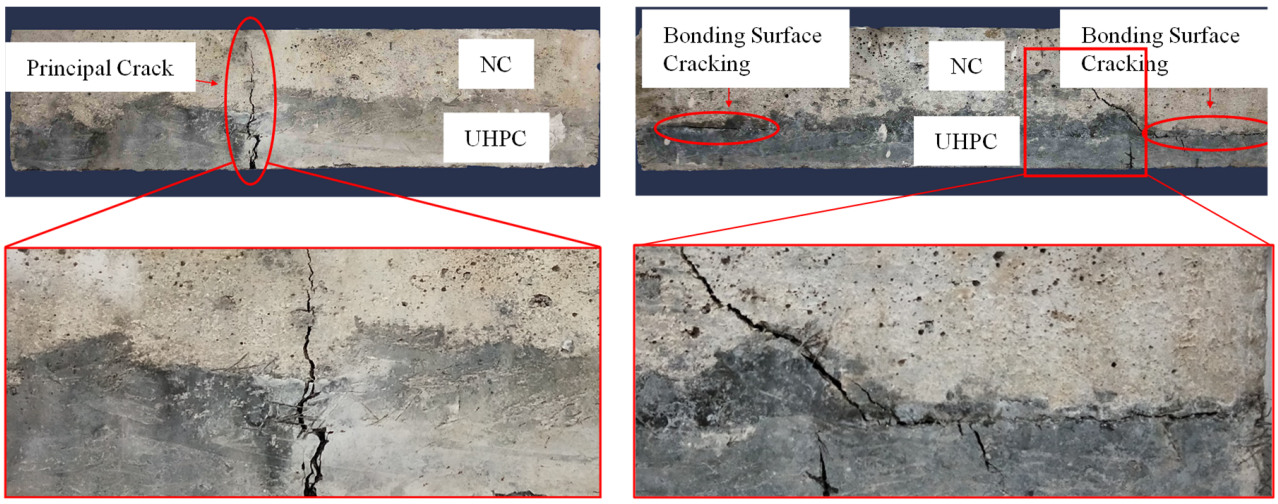

(**a**) Uncracked bonding surface (**b**) Bonding surface cracking

Figure 8. Classification of damage patterns of grooved specimens.

The distribution of the two damage modes of the groove-treated specimens is given in Figure 9. The proportion of type a (bonded surface without cracking) was larger, indicating that the UHPC–NC bonded surface is more reliable. The crack development pattern of the a-type damage was consistent with that of the overall bending and tensile specimens, indicating that the UHPC and NC can work together to coordinate the forces. The NC part of the b-type damage specimen showed shear damage cracks, while the UHPC part had not been fully functional, indicating that the two are not jointly stressed. This proved that the reliability of the bond surface played a decisive role in the damage pattern of the bending and tension of the composite specimens.

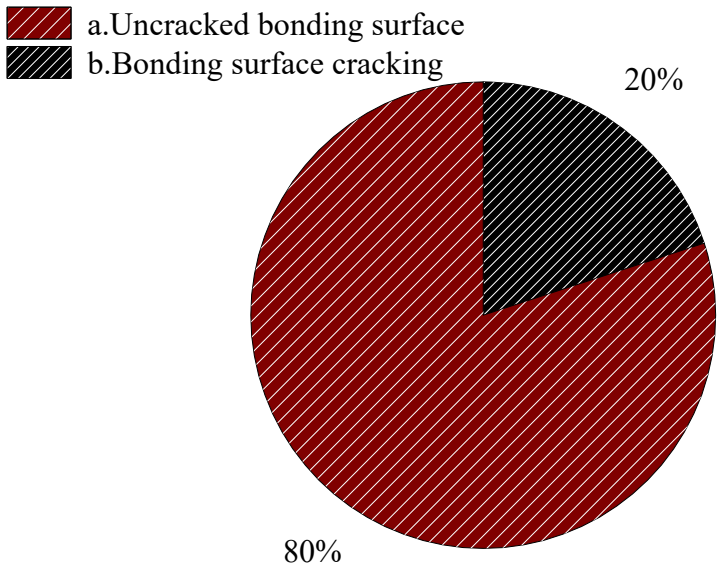

Figure 9. Distribution of damage patterns of grooved specimens.

(2) Paste group

Cracks developed upward from the lower edge of the UHPC and NC simultaneously. The damage to the bottom edge of the specimens occurred in the area between the two concentrated load lines. The damage pattern is shown in Figure 10. This indicated that the UHPC and NC were stressed separately due to the weak adhesive interface which did not coordinate the forces on the UHPC and NC portions together.

Figure 10. Damage mode of bonded group specimens.

(3) Pure NC and UHPC

The damage modes of pure NC and UHPC are shown in Figure 11. Pure NC developed damage rapidly after the appearance of initial cracks, showing obvious brittleness. In contrast, after the initial crack appeared in pure UHPC, it was constrained by steel fibers and developed more slowly, demonstrating obvious toughness. During the crack expansion process, the crisp sound of steel fibers being pulled out was heard, indicating that the failure mode was fiber and matrix bond failure rather than fiber fracture failure.

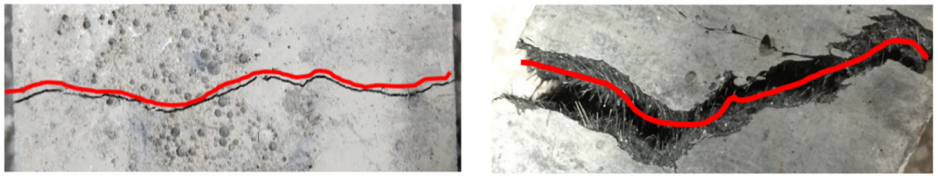

(**a**) Cracks for pure NC (**b**) Cracks for pure UHPC

Figure 11. Damage mode of pure NC and UHPC.

3.2. Load–Deflection Relationship

To evaluate the toughening effect of UHPC on UHPC–NC bending, the load–deflection curves during the test were plotted according to the test data. To facilitate the comparison, the average results for each group were selected for analysis, as shown in Figure 12.

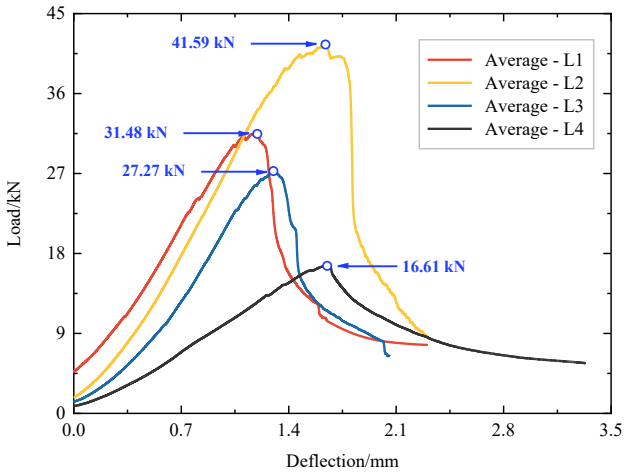

(**a**) UHPC–NC bending and tensile specimens

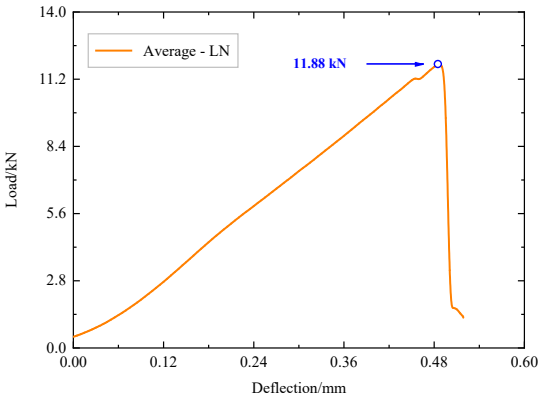

(**b**) Pure NC

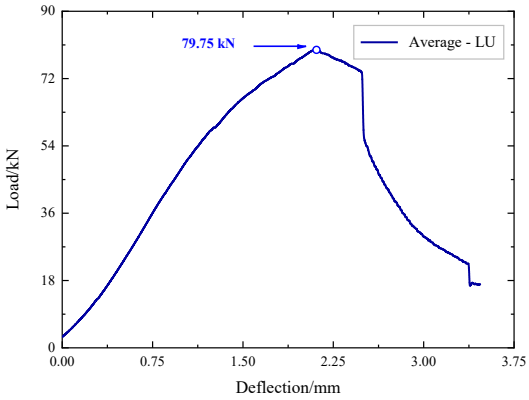

(**c**) Pure UHPC

Figure 12. Load–deflection curve of bending and strain specimens.

There are various specific evaluation methods for bending toughness, such as the strength method, the energy ratio method, and the deformation ratio method. Considering the effects of test conditions and other factors, this paper adopted the method recommended by the Japanese Society of Civil Engineers for the evaluation of bending tests. The energy absorbed by the specimens during the damage course was obtained via integration of the load–deflection curves. This energy was used to calculate the bend-tension toughness indicator, a commonly used method for evaluating the bending toughness of concrete.

The JSCE SF4 method is a strength method which is shown in Figure 13 and Equation (4). The method specified that the bending toughness coefficients were calculated using parameters such as the area enclosed by the load–deflection curve at deflection deformations up to 1/150 of the specimen span and the specimen dimensions.

$$\overline{\sigma} = \frac{T_b}{\delta_{tb}} \cdot \frac{l}{bh^2} \tag{4}$$

where $\overline{\sigma}$ was the bending and tensile toughness coefficient (MPa); δ_{tb} was the set deflection value, $\delta_{tb} = 20$ mm; T_b was the load–deflection curve with $x = \delta_{tb}$, the area surrounded by the axis; l was the specimen span; b was the specimen cross-section width; and h was the specimen cross-section height.

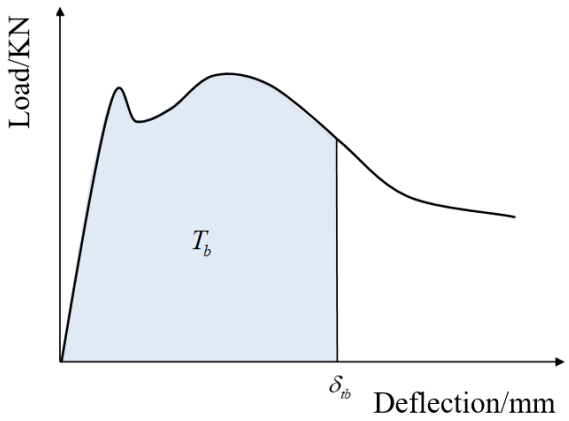

Figure 13. Schematic diagram of JSCE SF4 bending toughness evaluation methods.

In the elastic phase, the slope of the load–deflection curve indicated the stiffness of the specimen in this phase (the size of the load required to produce a unit of deflection, in kN/mm). The slope value was obtained by one-way linear regression on the linearly increasing part of the load–deflection curve. The area enclosed by the curve and the $x = 2$, x-axis was obtained by integration. The bending toughness coefficients were calculated using Equation (4). The calculation results are listed in Table 7 and Figure 14.

Table 7. Calculation parameters of load–deflection curves.

Specimen Number	Load/kN	Slope of the Elastic Segment	T_b/N·mm	$\overline{\sigma}$/MPa
L1	31.48	24.28	33.13×10^3	4.97
L2	41.59	26.82	46.25×10^3	6.94
L3	27.27	19.18	26.38×10^3	3.96
L4	16.61	10.15	18.56×10^3	2.78
LN	11.88	24.73	/	/
LU	79.75	47.52	89.24×10^3	13.39

Note: Since the toughness of the pure NC specimen is very low, LN-1 reached the destructive load without a ductile drop section. The measured deflection was less than the deflection value set by the calculation formula, so no calculation will be conducted.

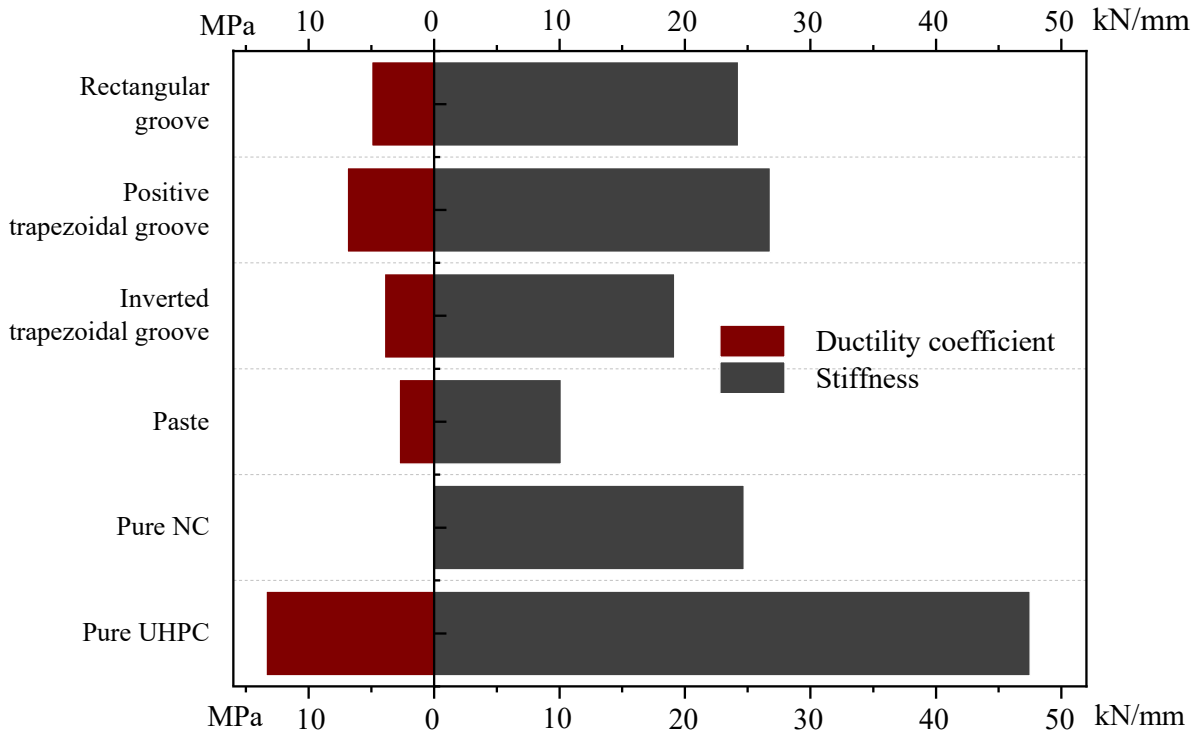

Figure 14. Toughness coefficient and stiffness.

Analyzing Figure 14, it can be seen that the stiffness of pure UHPC in the elastic phase was about two times that of pure NC. For the UHPC–NC composite specimens, the stiffness with interface adhesive treatment was the lowest, which was less than half of the stiffness of the pure NC. The interface-positive trapezoidal groove processed specimen exhibited the highest stiffness. The difference in stiffness between the interface-positive trapezoidal groove processed specimen and the pure NC specimen was not significant, indicating that the interface treatment type has a greater impact on the stiffness of UHPC–NC composite specimens.

The bending toughness coefficient reflected the toughness performance and the lower bending toughness coefficients indicated lower toughness. For the UHPC–NC composite specimens, the interface paste treatment of the specimen toughness was the worst, with only 21% of the pure UHPC toughness. The specimen with positive trapezoidal grooving at the interface had the best toughness and could reach 52% of the pure UHPC toughness. It was twice as high as that of the specimen with interface paste treatment, showing that the interface treatment also has a great influence on the toughness of the UHPC–NC composite structure.

3.3. Bending Tensile Strength Analysis

The ultimate load was recorded after the specimen was damaged. The bending strength was calculated according to Equation (5).

$$f_t = \frac{Fl}{bh^2} \tag{5}$$

where F was the breaking load (N); l was the specimen span (mm); b was the specimen section width (mm); and h was the specimen section height (mm).

The results of the tests are presented in Table 8.

Table 8. Strength of UHPC–NC bending and tensile specimens.

Groups	Specimen Number	Loading/kN	Destructive Strength/MPa	Destructive Strength Value/MPa	Destructive Strength STD/MPa	Incipient Crack Load/kN	Initial Crack Strength/MPa	Value of Initial Crack Strength/MPa
L1	L1-1	31.48	9.44	9.76	1.37	22.63	6.79	6.90
	L1-2	38.56	11.57			26.99	8.10	
	L1-3	27.56	8.27			19.43	5.83	
L2	L2-1	41.59	12.48	12.48	0	34.41	10.32	10.32
L3	L3-1	27.27	8.18	8.18	0	22.98	6.89	6.89
L4	L4-1	16.61	4.98	4.94	0.36	13.30	3.99	3.96
	L4-2	18.56	5.57			14.85	4.45	
	L4-3	14.23	4.27			11.41	3.42	
LN	LN-1	11.88	3.56	4.08	0.44	11.17	3.35	3.83
	LN-2	13.46	4.04			12.64	3.79	
	LN-3	15.42	4.63			14.51	4.35	
LU	LU-1	79.75	23.93	25.33	1.66	59.04	17.71	20.00
	LU-2	92.21	27.66			76.67	23.00	
	LU-3	81.29	24.39			64.22	19.27	

Note: Define the strength value as the average value of the strength data of the same group of three specimens.

The initial cracking load in this test was also equivalent to the elastic limit load because of the low tensile capacity of plain concrete, which will crack once the elasticity phase is over. The values of the initial cracking strength and failure strength of each group of specimens are plotted as shown in Figure 15.

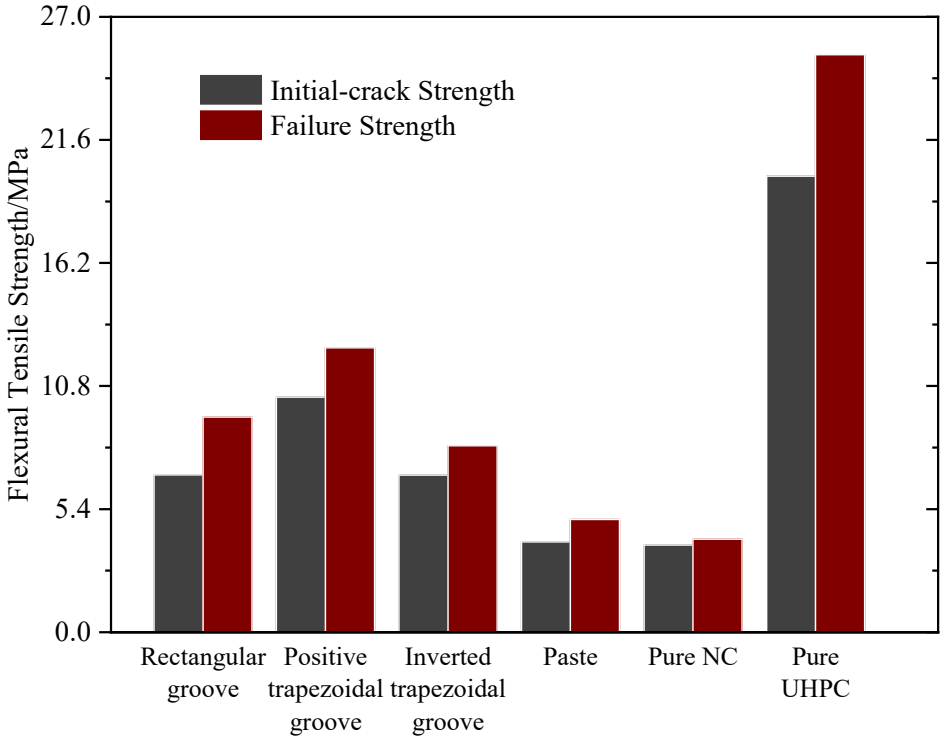

Figure 15. Relationship between test factors and bending strength.

Analyzing Figure 15 and Table 8, it can be seen that the bending strength of pure NC specimens was extremely low. The initial cracking strength was almost equal to the ultimate strength, indicating that pure NC specimens exhibited brittle damage. The bending strength of pure UHPC specimens can be up to six times the bending strength of pure NC. The increase from initial crack strength to ultimate strength was larger, indicating that pure NC specimens exhibited ductile damage. The steel fibers contributed the strength and toughness of UHPC. The bending strength of UHPC–NC composite specimens was between that of UHPC and NC. The increase in initial crack strength to ultimate strength

was also between the two, similar to the bending strength of pure NC specimens. The specimens with interfacial trapezoidal NC groove treatment had the highest strength, which was about double that of pure NC specimens. The strength of the interface right-angled and inverted trapezoidal groove-treated specimen was lower, but it was still about twice as high as that of the pure NC specimen. This is because the inverted trapezoidal groove, when subjected to a tensile component perpendicular to the beveled edge of the groove, would lead to shear cracks toward the bond interface, resulting in increased cracking of the bonded surface. While the positive trapezoidal beveled groove was subjected to a tensile component perpendicular to the beveled edge of the cut groove, the shear cracks progressed toward the interior of the matrix [35]. The bond surface was prevented from inhibiting premature cracking, thus improving the bond tensile performance as shown in Figure 16.

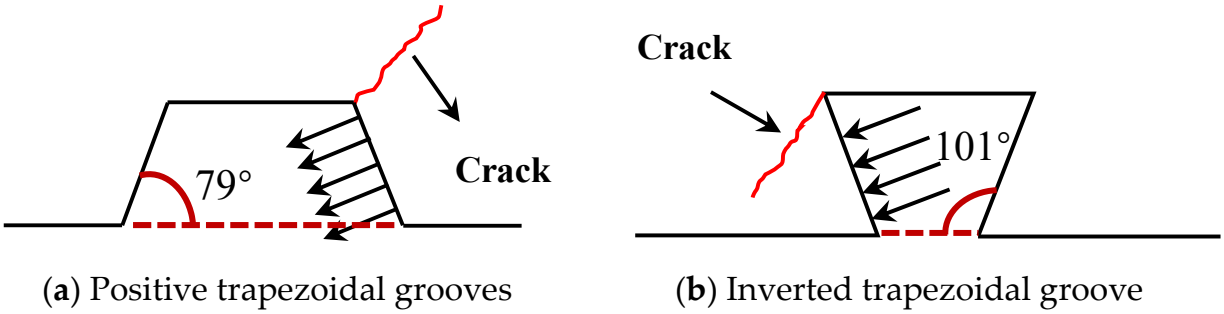

Figure 16. Schematic diagram of groove cracking.

This result showed that the interface treatment has a more obvious effect on the strength of the UHPC–NC composite. The performance improvement effect of interfacial paste treatment was very low, whereas the interface-positive trapezoidal groove treatment effectively improved the interface bending performance.

4. Finite Element Modeling

ANSYS [2023 R2 version] is a finite element computing software commonly used in bridge engineering with large modeling capability, strong solution capability, excellent nonlinear analysis capability, and good optimization capability. It is an important tool for engineers and researchers carrying out research. In this paper, ANSYS finite element software will be used to simulate the UHPC–NC bending specimens.

4.1. Material Constitutive

The model used SOLID65 solid cells to simulate UHPC and NC. The detailed material performances are shown in Table 9. In the finite element model, the multilinear isotropic strengthening model (MISO model) was used to establish the material constitutive relationship between UHPC and NC. The stress–strain relationship was described by a multi-segment straight line. The damage criterion used the isotropically strengthened MISS yield criterion. The rising segment of the curve was obtained from the UHPC material properties test. The horizontal segment was used in some of the references after the peak value. The constitutive stress–strain relationship of UHPC is shown in Figure 17.

Table 9. UHPC and NC material properties.

	Modulus of Elasticity	Yield Strength	Poisson's Ratio
UHPC	45 GPa	114.9 MPa	0.2
NC	32.5 GPa	40 MPa	0.2

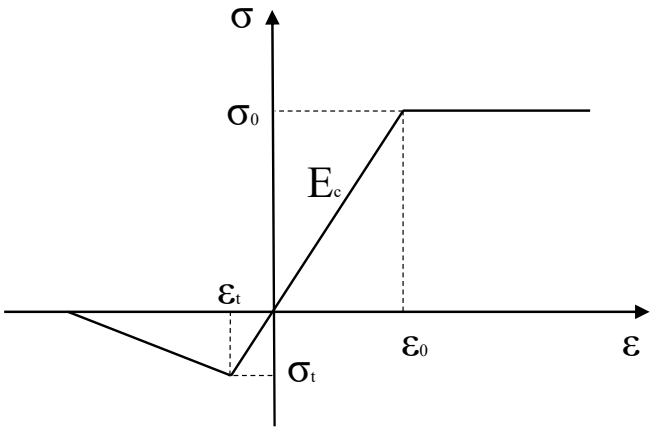

Figure 17. Stress–strain relationship of UHPC.

4.2. Bonding Interface Parameters

To aptly simulate the test model, it was necessary to consider the existence of the bond-slip phenomenon between the UHPC and the NC. Hence, it was necessary to use the connection unit between the UHPC and the NC. The frequently used connection units are the spring unit and the contact unit. Referring to the literature, this paper chose to use the nonlinear spring unit COMBINATION39 to simulate the bond-slip phenomenon at the interface between UHPC and NC. The stiffness matrix for the COMBINATION39 cell is shown in Equation (6). The cell node load vectors are shown in Equation (7).

$$[k]^e = \mathrm{k}_{tg}\begin{bmatrix} 1 & -1 \\ -1 & 1 \end{bmatrix} \tag{6}$$

$$[F]^e = \mathrm{F}\begin{bmatrix} 1 \\ -1 \end{bmatrix} \tag{7}$$

where k_{tg} was the stiffness coefficient of the spring unit, the value could be obtained from Figure 18.

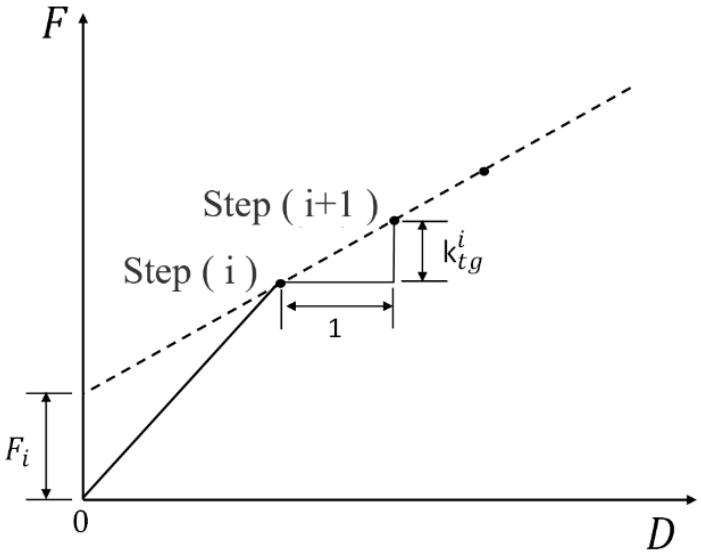

Figure 18. Schematic diagram of spring unit stiffness coefficient values.

In the finite element model, each pair of nodes on the UHPC–NC bonding surface was connected by a spring unit. The interaction in the vertical direction of the bonding

surface was indicated by the setting of real constants. Each spring unit has no length, and its performance was defined by the load–deflection curve of the spring.

According to the actual size of the specimen to establish the bending model, the model defined the horizontal longitudinal direction as the x-direction, and the bond interface normal direction as the y-direction. To save calculation time, the bending model was selected to analyze the four cases of interface right-angled grooves, inverted trapezoidal grooves, positive trapezoidal grooves, and interface bonding. The bending model is shown in Figure 19.

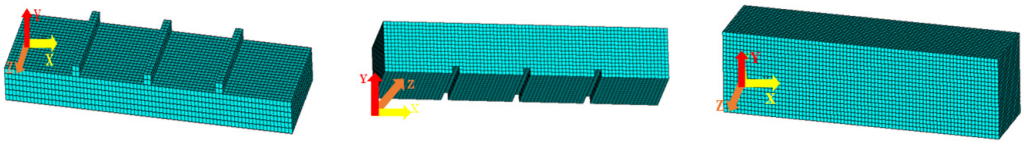

(**a**) NC component (**b**) UHPC component (**c**) Bending

Figure 19. Bending finite element model.

4.3. Comparative Analysis of Experiments and Finite Elements

4.3.1. UHPC–NC Bond Constraint Shrinkage Modeling Analysis

Shrinkage produced by freshly cast UHPC was modeled by the equivalent temperature difference method in this article. The principle of the equivalent temperature difference method to simulate shrinkage was the initial strain method, i.e., based on the principle that the deformation produced by shrinkage was equal to the deformation produced by temperature change. Shrinkage was equated to a temperature difference, and the temperature load was applied to the freshly cast concrete to achieve the same effect of shrinkage. The coefficient of linear expansion was an indispensable parameter for temperature equivalence. The coefficient of linear expansion of UHPC used in this paper was 11.76 με/°C. UHPC shrinkage was taken as the final shrinkage strain of 360με measured in the shrinkage test in Section 2.2.1. Since the paste group model did not need to consider the effect brought about by the contraction of UHPC, it was chosen to apply the temperature load to the model of the bending groove group for calculation. The horizontal stress clouds of the NC, UHPC, and UHPC–NC composite specimens of the model are shown in Figure 20.

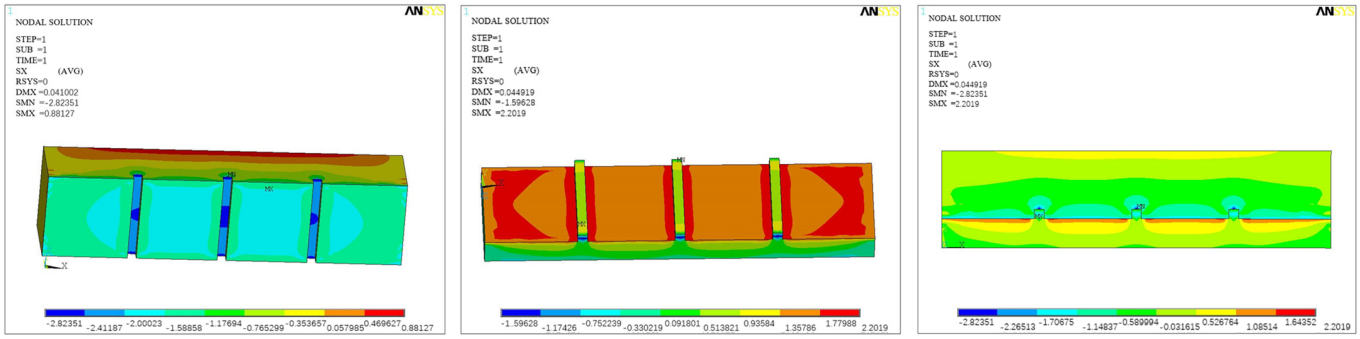

(**a**) NC (**b**) UHPC (**c**) Bending model

Figure 20. Right-angled slot bending model (horizontal direction).

From Figures 20–22, it can be seen that for the bonded interface, the UHPC side was mainly subjected to tensile stresses while the NC side was mainly subjected to compressive stresses. In the vertical direction of the model, the tensile stress in the UHPC portion was largest at the bonding surface, and gradually decreasing to zero towards the edge of the model, and then transforming into the compressive stress. The position where the tensile stress was zero was not subjected to confining stress, meaning it was free from shrinkage. In contrast, the shrinkage of UHPC at the bonding surface was subjected to the NC confining limiting effect, resulting in tensile stress. The stress distribution on the bonding surface on

the UHPC side was not even, and the phenomenon of stress concentration occurred. Tensile stress distribution tends to be great on both sides and low in the middle. The stress at the groove position was the lowest. This indicated that if the bonding surface was not strong enough, the end of the bonding surface may be the first to experience shrinkage cracking. This led to the destruction of the bonding surface, and it was very unlikely that shrinkage cracking would occur first at the groove. This was consistent with the damage that occurs in actual strengthening projects, especially when the freshly poured concrete was a thin layer, and the UHPC strengthening was particularly suitable for thin-layer strengthening, demonstrating the accuracy of the finite element model.

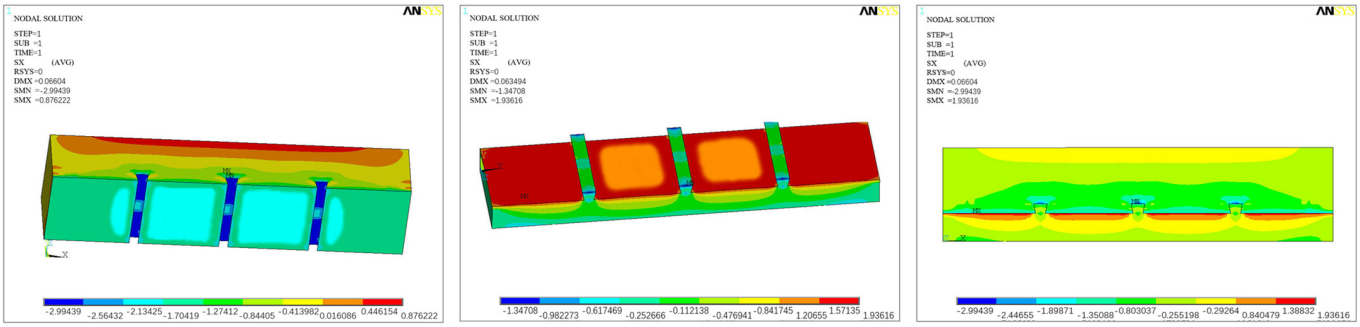

(**a**) NC (**b**) UHPC (**c**) Bending model

Figure 21. Stress cloud diagram of inverted trapezoidal groove bending model.

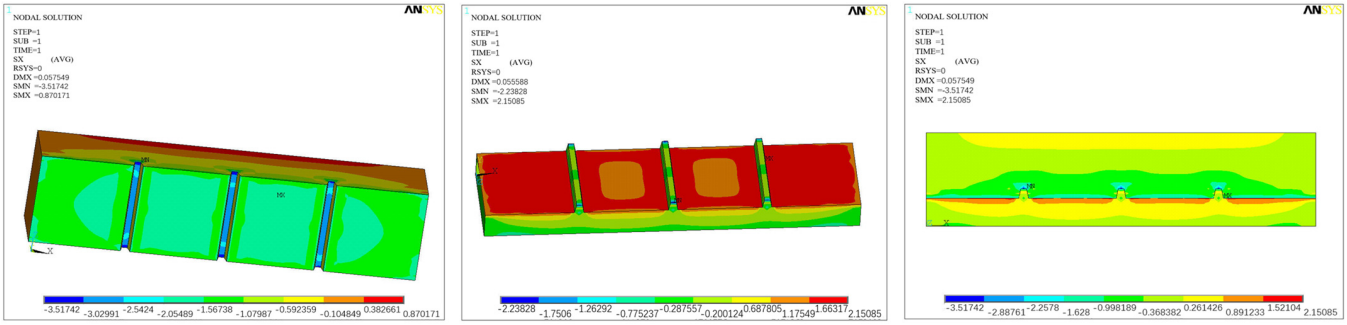

(**a**) NC (**b**) UHPC (**c**) Bending model

Figure 22. Stress cloud diagram of positive trapezoidal groove bending model.

UHPC (tensile strength $\geq$ 10 MPa) can achieve a tensile strength five times greater than that of NC. The maximum tensile stress appearing in the model calculation results was 2.2 MPa, which was far from the UHPC cracking strength. It has been observed that using the measured values of elastic modulus and free shrinkage values to calculate the shrinkage stresses, can lead to higher results compared with the measured values of shrinkage stresses. So, this showed that the risk of UHPC constrained shrinkage cracking was very low.

By comparing the maximum tensile stress values of right-angled grooves, inverted trapezoidal grooves, and positive trapezoidal grooves, it is found that there was little difference among the three, indicating that the form of grooving did not have a significant effect on the restraining shrinkage stresses.

4.3.2. UHPC–NC Bonded Slip Model Analysis

To investigate the effect of different bond interface treatments on the stress distribution of specimens, the same load was applied to different models to control a single variable.

The same load of 25 kN was applied to each bending model. The horizontal longitudinal stress clouds of the NC, UHPC, and the composite specimens are shown in Figure 23.

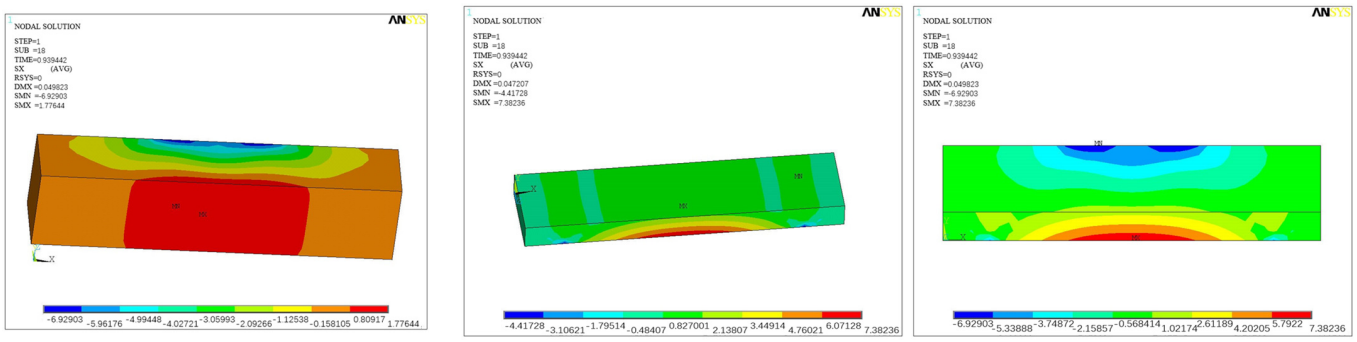

(**a**) NC (**b**) UHPC (**c**) Bending model

Figure 23. Paste bending model.

From Figures 23–26, it can be seen that for the bonding interface of the pure bending section, both NC and UHPC were mainly subjected to tensile stresses, and no compressive stresses occurred. For the UHPC–NC bending model as a whole, NC was mainly subjected to compressive stress, which decreased gradually from the loading surface to the bonding interface. UHPC was mainly subjected to tensile stress, which decreased gradually from the bottom surface of the model to the bonding interface. For the x-direction of the model, the stress distribution tended to be the greatest in the middle of the model span and became increasingly smaller on both sides. This indicated that the specimen would be damaged near the middle of the span in the context of strong interfacial bonding. This was consistent with the damage pattern of the specimen without cracking on the bonding surface. The damaged area on the lower bottom surface of the specimen appeared in the range within the two loading points.

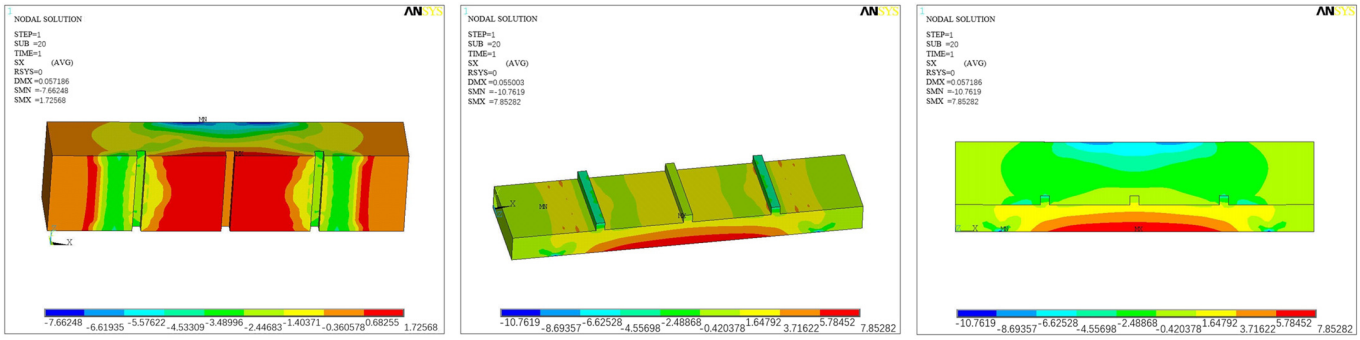

(**a**) NC (**b**) UHPC (**c**) Bending model

Figure 24. Right-angled slot bending model (vertical direction).

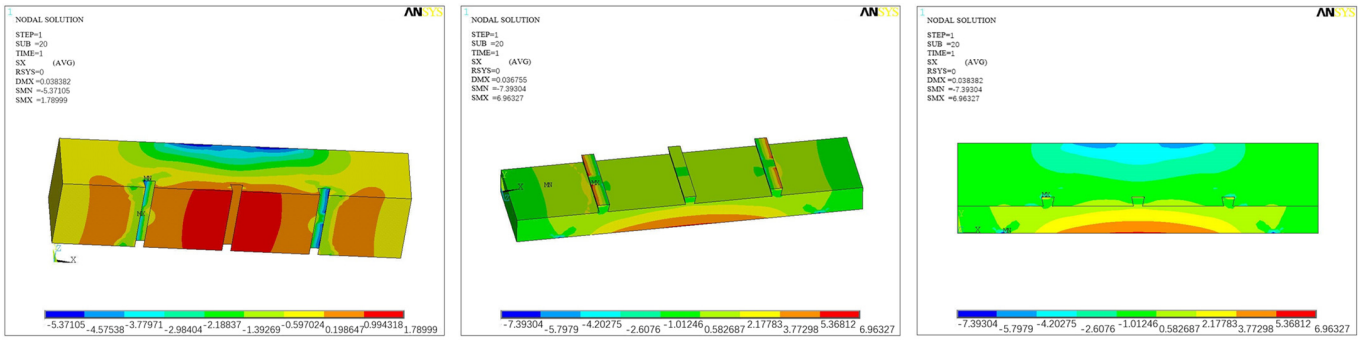

(**a**) NC (**b**) UHPC (**c**) Bending model

Figure 25. Inverted trapezoidal groove bending model.

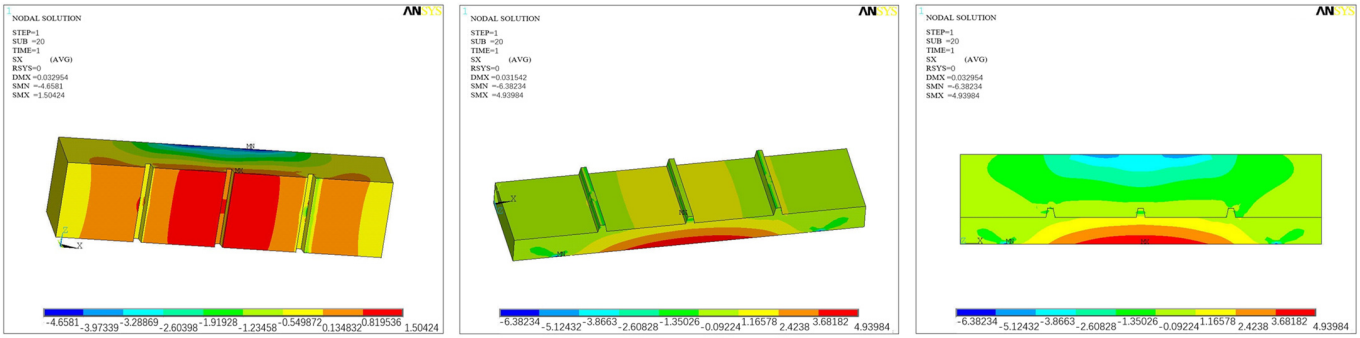

(**a**) NC (**b**) UHPC (**c**) Bending model

Figure 26. Positive trapezoidal groove bending model.

Although the bonded interfaces of different treatments were all mainly subjected to tensile stresses, the different treatments affected the distribution of tensile stresses at the bonded interfaces. For the pasted model, the tensile stress distribution on the bonding surface of the pure bending section was relatively uniform. The stress distributions of the right-angled groove model, inverted trapezoidal groove model, and pasted model were similar. The pressure values were not so different. For the positive trapezoidal groove model, the tensile stress on the NC side of the bonding surface was reduced by about 15% compared to the other models at the same location, indicating that the presence of the positive trapezoidal groove weakened the tensile stress on the NC side of the bonding surface, which was beneficial to the composite structure. This was also in agreement with the results obtained in the tests which highlight that the interfacial bond bending performance of the positive trapezoidal groove specimens was optimal. This indicated that the finite element model has a certain degree of accuracy.

5. Conclusions

Two types of UHPC–NC interfacial bonding, grooving treatment, and epoxy bonding, were considered to investigate the bending performance of UHPC-reinforced concrete structures. By organizing and analyzing the results and finite element calculation of the bonding model, the following main conclusions are presented:

- UHPC completed shrinkage under steam-conditioned conditions ahead of schedule, 80% ahead of the non-steam-conditioned UHPC at the same age. The UHPC–NC bond-constrained shrinkage ANSYS model calculations showed that the risk of UHPC-constrained shrinkage cracking was very low. The shrinkage stresses on the UHPC side bond interface showed a distribution with two large sides and a small middle, with the minimum stress at the notch location.
- The NC groove width factor had the most significant effect on the rate of strength loss of the NC matrix and the bond shear strength of the UHPC–NC interface. Groove widths of $\leq$ 20 mm and NC groove volume loss rates of $\leq$ 0.06% were recommended. The relationship equation between the NC matrix volume loss rate and interfacial bond shear strength was summarized to provide a quantitative reference basis for matrix groove treatment.
- The damage pattern of the bonded surface in the bending and tension specimens only accounted for 22.2%. The UHPC–NC bonded surface was very reliable. The failure mode of UHPC–NC bond interface was closely related to the bond strength.
- The UHPC–NC interface shear bond-slip curves went through an elastic rise phase, a yielding phase, and a destructive fall phase, and some of the curves had no yielding phase. Overall, the slip corresponding to the ultimate interfacial bond strength was small, all below 0.8 mm. Most of the bonded interface damage was brittle, with about 20% of the specimens showing some ductile characteristics. This indicated that UHPC improves the toughness of the bonded interface.

- The bonding performance of the grooving interface was better than that of the bonding interface. The interface bonding shear strength of the grooving group was about 2 times higher than that of the pasting group. The bending performance of the paste group test was very poor, and the UHPC and NC could not coordinate forces.
- Calculations from the ANSYS model showed that the grooving treatment was able to transfer the large stress region from the NC to UHPC side, which was beneficial to the strengthening structure. The maximum tensile stress reduction on the NC bonding surface of the positive trapezoidal groove model was consistent with the test results indicating that the finite element model analysis results were reliable.

Author Contributions: Investigation, C.Z.; resources, C.Z.; writing—original draft, Y.F.; software, J.T.; validation, J.T. and J.Y.; writing—review and editing, Z.J.; methodology, Z.J.; funding acquisition, Y.L.; formal analysis, Y.L.; supervision, J.Y. All authors have read and agreed to the published version of the manuscript.

Funding: This research was funded by financial support from the Technology Project of Transportation Department of Guizhou Province, grant number 2024-122-001.

Data Availability Statement: The raw data supporting the conclusions of this article will be made available by the authors on request.

Conflicts of Interest: Authors Chao Zhu and Jie Tang are employed by the Chongqing Design Group Co., Ltd. Author Yinbin Li is employed by the Guizhou Provincial Transportation Planning Survey and Design Institute Co., Ltd. The remaining authors declare that the research was conducted in the absence of any commercial or financial relationships that could be construed as a potential conflict of interest.

References

1. Richard, P.; Cheyrezy, M. Reactive powder concretes with high ductility and 200–800 MPa compressive strength. In *Conc Tech: Past, Present, Future, ACI*; Special Publication: Madison, WI, USA, 1994; Volume 114, pp. 507–518.
2. Wang, D.; Shi, C.; Farzadnia, N.; Jia, H.; Zeng, R.; Wu, Y.; Lao, L. A quantitative study on physical and chemical effects of limestone powder on properties of cement pastes. *Constr. Build. Mater.* **2019**, *204*, 58–69. [CrossRef]
3. Habert, G.; Denarié, E.; Šajna, A.; Rossi, P. Lowering the global warming impact of bridge rehabilitations by using Ultra High Performance Fibre Reinforced Concretes. *Cem. Concr. Compos.* **2013**, *38*, 1–11. [CrossRef]
4. Yu, R.; Spiesz, P.; Brouwers, H.J.H. Mix design and properties assessment of Ultra-High Performance Fibre Reinforced Concrete (UHPFRC). *Cem. Concr. Res.* **2014**, *56*, 29–39. [CrossRef]
5. Ttmann, F. *Adherence of Young on Old Concrete*; Aedificatio Publishers Freiburg: Breisgau, Germany, 1994.
6. Bartolozzi, M.; Casas, R.J.; Domaneschi, M. Bond deterioration effects on corroded RC bridge pier in seismic zone. *Struct. Concr.* **2022**, *23*, 51–66. [CrossRef]
7. Hantouche, G.E.; Harajli, M.; Haddadin, F.; Elsouri, A. Seismic Strengthening of Bond-Critical Regions in Wall-Type Bridge Piers Using Active Confinement. *J. Bridge Eng.* **2015**, *20*, 04015002. [CrossRef]
8. Leng, J.; Yang, J.; Zhang, Z.; Du, J.; Zou, Y.; Zhou, J. Effect of vehicle-induced vibration on the strength, nano-mechanical properties, and microstructural characteristics of ultra-high-performance concrete during hardening process. *Cem. Concr. Compos.* **2024**, *148*, 105487. [CrossRef]
9. Lu, W.L.; Peng, W.Q.; Zhu, L.; Ma, B.; Li, F.-L. Study on mechanical behavior of steel-UHPC-NC composite beams under negative bending moment. *Case Stud. Constr. Mater.* **2022**, *17*, e01593. [CrossRef]
10. Tong, T.; Yuan, S.; Wang, J.; Liu, Z. The role of bond strength in structural behaviors of UHPC-NC composite beams: Experimental investigation and finite element modeling. *Compos. Struct.* **2021**, *255*, 112914. [CrossRef]
11. Li, X.; Hu, Z. Cracking Resistance of UHPC-NC Structure in Negative Moment Zone of Prestressed Concrete Beam Bridges. *Arab. J. Sci. Eng.* **2023**, *48*, 4795–4804. [CrossRef]
12. Li, Y.; Zhou, H.; Zhang, Z.Z.; Yang, J.; Wang, X.; Zou, Y. Macro-micro investigation on the coefficient of friction on the interface between steel and cast-in-place UHPC. *Eng. Struct.* **2024**, *318*, 118769. [CrossRef]
13. Zhang, Z.; Zou, Y.; Yang, J.; Zhou, J. Capillary rise height of sulfate in Portland-limestone cement concrete under physical attack: Experimental and modelling investigation. *Cem. Concr. Compos.* **2022**, *125*, 104299. [CrossRef]
14. Zhang, Z.; Pang, K.; Xu, L.; Zou, Y.; Yang, J.; Wang, C. The bond properties between UHPC and stone under different interface treatment methods. *Constr. Build. Mater.* **2023**, *365*, 130092. [CrossRef]
15. Lampropoulos, A.P.; Paschalis, S.A.; Tsioulou, O.T.; Dritsos, S.E. Strengthening of reinforced concrete beams using ultra high performance fibre reinforced concrete (UHPFRC). *Eng. Struct.* **2016**, *106*, 370–384. [CrossRef]
16. Habel, K.; Viviani, M.; Denarié, E.; Brühwiler, E. Development of the mechanical properties of an Ultra High Performance Fiber Reinforced Concrete (UHPFRC). *Cem. Concr. Res.* **2006**, *36*, 1362–1370. [CrossRef]

17. Chen, R.; Zhang, Z.; Zou, Y.; Yang, J.; Zhou, J.; Kuang, Y.; Wang, Y. In-situ evaluation on existing RC beam strengthened with GFRP-reinforced UHPC overlay. *Constr. Build. Mater.* **2024**, *429*, 136363. [CrossRef]
18. Farhat, F.A.; Nicolaides, D.; Kanellopoulos, A.; Karihaloo, B. High performance fibre-reinforced cementitious composite (CARDIFRC)–Performance and application to retrofitting. *Eng. Fract. Mech.* **2007**, *74*, 151–167. [CrossRef]
19. Beschi, C.; Meda, A.; Riva, P. Column and Joint Retrofitting with High Performance Fiber Reinforced Concrete Jacketing. *J. Earthq. Eng.* **2011**, *15*, 989–1014. [CrossRef]
20. Yang, J.; Xia, J.; Zhang, Z.; Zhou, J.; Zou, Y.; Wang, Y.; Shen, X. Mesoscopic shear behavior and strength characteristic of UHPC-NC interface considering the combined effect of mechanical interlocking and dowel action. *Eng. Fract. Mech.* **2024**, *307*, 110306. [CrossRef]
21. Tayeh, B.A.; Bakar, B.H.A.; Johari, M.A.M.; Zeyad, A. Microstructural analysis of the adhesion mechanism between old concrete substrate and UHPFC. *J. Adhes. Sci. Technol.* **2014**, *28*, 1846–1864. [CrossRef]
22. Tayeh, B.A. Evaluation of Bond Strength between Normal Concrete Substrate and Ultra High Performance Fiber Concrete as a Repair Material. *Procedia Eng.* **2013**, *54*, 554–563. [CrossRef]
23. Carbonell, M.; Harris, D.; Shann, S.; Ahlborn, T.M. Bond Strength between UHPFRC and Normal Strength Concrete (NSC) in Accordance with Split Prism and Freeze-Thaw Cycling Tests. In Proceedings of the Hipermat, 3rd International Symposium on UHPC and Nanotechnology for High Performance Construction Materials, Kassel, Germany, 7–9 March 2012.
24. Sarkar, J. Characterization of the Bond Strength between Ultra High Performance Concrete Bridge Deck Overlays and Concrete Substrates. Ph.D. Thesis, Michigan Technological University, Houghton, MI, USA, 2010.
25. Alhallaq, A.F.; Tayeh, B.A.; Shihada, S. Investigation of the Bond Strength Between Existing Concrete Substrate and UHPC as a Repair Material. *Int. J. Eng. Adv. Technol.* **2017**, *6*, 210–217.
26. Li, Z.; Rangaraju, P.R. Investigation into Flexural Bond Strength Test Method to Evaluate Influence of Surface Roughness on Bond Characteristics of UHPC with Precast Concrete. In Proceedings of the International Interactive Symposium on UHPFRC, Des Moines, IA, USA, 18–20 July 2016.
27. Alaee, F.J.; Karihaloo, B.L. Retrofitting of reinforced concrete beams with CARDIFRC. *J. Compos. Constr.* **2003**, *7*, 174–186. [CrossRef]
28. Tayeh, B.A.; Bakar, B.H.A.; Johari, M.A.M.; Zeyad, A. Flexural Strength Behavior of Composite UHPFC—Existing Concrete. *Adv. Mater. Res.* **2013**, *701*, 32–36.
29. Eisaigh, W.A.; Robberts, J.M.; Kearsley, E.P. Modeling the behavior of steel-fiber reinforced concrete ground slabs. I: Development of material model. *J. Transp. Eng.* **2011**, *137*, 882–888. [CrossRef]
30. Tz-cornelius, M.; Pahn, M. Investigations on the size effect of thin structural elements made of UHPC. In Proceedings of the 4th International Symposium on Ultra-High Performance Concrete and High Performance Construction Materials, Kassel, Germany, 9–11 March 2016; pp. 1–11.
31. Beushausen, H. A parameter study on the age at cracking of bonded concrete overlays subjected to restrained shrinkage. *Mater. Struct.* **2015**, *49*, 1905–1916. [CrossRef]
32. Li, C.; Ji, D.L.; Zhang, D.; Chen, B. Pull-out test of hybrid connection in steel-UHPC composite slab. *Structures* **2024**, *66*, 106832. [CrossRef]
33. Zhang, S.; Lv, G.; Ma, F.; Wang, Z.; Liu, Y. Influence of Contact Interface Friction on Plastic Deformation of Stretch-Bend Forming. *Coatings* **2022**, *12*, 1043. [CrossRef]
34. *GB/T 50082-2009*; Introduction of Revised Standard for Test Methods of Long-term Performance and Durability of Ordinary Concrete. Ministry of Housing and Urban-Rural Development, PRC: Beijing, China, 2010.
35. Liu, H.; Wang, H.; Zhang, Y.; Liu, X. Shear resistance of UHPC connection for prefabricated reinforced concrete slabs with shear grooves and dowel rebars. *Constr. Build. Mater.* **2024**, *454*, 139153. [CrossRef]